Evanescent Field Raman Scattering by Roton-Type Excitations

Anatoly Kuklov, Alexei Bulatov, and Joseph L. Birman
Department of Physics, The City College of the City University of New York, New York, New York 10031
(Received 4 January 1994)

Evanescent field Raman scattering of light is proposed as a method for probing roton-type peculiarities of the excitation spectrum of 2D electron gas in a strong magnetic field. These peculiarities are essential for the modern theories of the fractional quantum Hall effect. We predict the magnetoroton contribution to be comparable to the intensity, measured in the conventional backscattering geometry. This method may also be applied to 3D samples, exhibiting the roton-type spectrum of quasiparticles. Particularly, in the familiar case of rotons in liquid ^{4}He, we show that the contribution of evanescent field Raman scattering by rotons is expected to be comparable to the Mandelstam-Brillouin contribution.

PACS numbers: 73.40.Hm, 67.40.Db, 78.30.−j

One of the most evident manifestations of the cooperative phenomena in condensed matter physics are the roton-type collective excitations, first predicted by Landau for ^{4}He (see [1]). Some time ago, it was realized that a similar kind of phenomenon should also occur in the 2D electron gas, subjected to a strong magnetic field [2]. In [3] it was suggested that using the roton-type peculiarities of the excitation spectrum will be a test of the modern theories of the fractional quantum Hall effect. We recall that incommensurate structural transitions in a solid are also preceded by softening of the excitation spectrum at some finite wave vector [4]. Therefore, the study of roton-type excitations is quite important for understanding cooperative phenomena in condensed matter.

In the case of liquid ^{4}He, the roton wavelength λ_r is of the order of 10^{-8} cm. In the quantum Hall regime, λ_r is expected to be of the order of the typical magnetic length, $\lambda_H \cong 10^{-6}$ cm [2,3]. Most of the spectral peculiarities of incommensurate transitions also occur in the mesoscopic range of wavelength, 10^{-6}–10^{-7} cm. Therefore, since the typical wavelengths of laser radiation used in Raman scattering (RS) exceed 10^{-5} cm, the direct observation of rotons in the first-order RS experiments is impossible, unless some disorder cancels the wave vector conservation [5]. One should note that the RS by the pair of rotons (second-order process) in liquid helium has been observed in [6], where the total intensity was 10^{-3} times smaller than that of the Mandelstam-Brillouin line.

The method of near-field tunneling microscopy [7] proved to be useful in resolving features as small as a tenth of the light wavelength. The correlation photon spectroscopy from the region of an evanescent field was used to study interface relaxation phenomena in polymers [8].

In this paper, we will show that if the geometry of the evanescent field Raman scattering (EFRS) is suitably chosen, the roton-type peculiarity is observable as the first-order feature in the 2D electron gas as well as in ^{4}He, even if the wavelength of the roton is several orders of magnitude shorter than the wavelength of incident light. Therefore, the spatial resolution might be higher than in the method of near-field tunnel microscopy. This happens due to nonconservation of the normal component of the wave vector as well as the strong enhancement of density of states in the roton region of the spectrum.

Let us consider a simple geometry when the EFRS can take place from the region $z \geq a/2$, denoted as "the sample" (Fig. 1). In the 2D case, "the sample" should be replaced by the plane containing the 2D electron gas (2DEG) (see Fig. 2). For simplicity, we assume that one of the light modes propagates in a transparent "slab," located in the region $|z| \leq a/2$. We denote refractive indices of the "slab" and the medium n_1 and n_2, respectively. Then, $n_1/n_2 = n > 1$, $n = \sqrt{\varepsilon}$. The light, traveling in the slab $|z| \leq a/2$ with the wave vector $\mathbf{k}_y$, penetrates into the region $|z| > a/2$ for some finite length δ^{-1}.

For simplicity, let us assume that the light is polarized perpendicular to the (y,z) plane. Then, the electric field amplitude is

$$\begin{aligned} &E(y,z) \equiv E_x(y,z), \quad E_y = E_z \equiv 0, \\ &E(y,z) = E_0 e^{ik_y y} \cos(k_z z), \quad |z| \leq a/2, \\ &E(y,z) = E_0 e^{ik_y y} e^{\delta(a/2-|z|)}, \quad |z| \geq a/2. \end{aligned} \tag{1}$$

Maxwell's equations and boundary conditions give us

$$\begin{aligned} &k_z^2 + k_y^2 = \frac{\Omega^2}{c^2}\varepsilon, \quad k_z^2 + \delta^2 = \frac{\Omega^2}{c^2}(\varepsilon - 1), \\ &\frac{\delta}{k_z} = \tan\left(k_z \frac{a}{2}\right), \quad c \equiv \frac{c_0}{n}, \end{aligned} \tag{2}$$

where Ω stands for the frequency of the light traveling inside the slab and c_0 is the light velocity in vacuum.

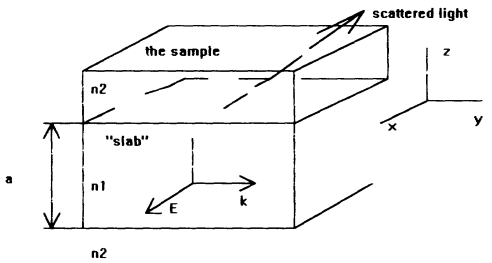

FIG. 1. The geometry for 3D EFRS.

In this paper we will only consider the bulk excitations created in the $|z| \geq a/2$ subspace which are characterized by the structure factor $S(q_z,\mathbf{q},\omega)$, $\mathbf{q}=(q_x,q_y)$, $\omega=\Omega-\Omega'$ with Ω' taken as the scattered photon frequency. Likewise, in the 2D geometry (Fig. 2) we consider the magnetoroton far from the AB edge. The role of boundary excitations between the slab and the sample will be considered elsewhere.

To obtain the nonresonant scattering intensity I, we employ the general procedure [9], assuming that the incident light produces a polarization

$$p_i(z,\mathbf{x},t)=\alpha_{ij}(z,\mathbf{x},t)E_j(z,\mathbf{x},\Omega), \quad z>a/2, \tag{3}$$

by means of the time-dependent polarization tensor α_{ij}. Let us consider diagonal RS, assuming that $\alpha_{ij}\sim\rho(z,\mathbf{x},t)\delta_{ij}$, where ρ stands for the density fluctuations in the sample. In case of small energy transfer, one finds [9]

$$I_{ij}(\omega)=C\int_0^{+\infty}dz\int_0^{+\infty}dz'\int d^2x\,d^2x'\int_{-\infty}^{+\infty}dt\,e^{-i\omega t}\langle\alpha(z,\mathbf{x},t)\alpha(z',\mathbf{x}',0)\rangle \times E_i(z,\mathbf{x})E_j(z',\mathbf{x}')\exp[-ik'_\perp(z-z')-i\mathbf{k}'\cdot(\mathbf{x}-\mathbf{x}')], \tag{4}$$

with the factor C independent of ω and ρ. Hereafter, we will omit this unimportant factor. In (4), $k'_\perp,\mathbf{k}'$ stand for the normal and tangential scattered light wave vector components with respect to the boundary and $\langle\cdots\rangle$ means the thermodynamic average. In (4), we should take into account (1) and (2).

Now, let us consider the EFRS from the 2D electron system in a strong magnetic field. In this case, as we mentioned before, the sample looks like a plane (Fig. 2). The plane of the 2D electron gas is tilted by some angle β with respect to the slab, with the magnetic field being orthogonal to the plane. In this geometry ($\beta\neq0$), the roton moving in a plane is affected by a normal (nonconserving) component of the momentum transfer of light.

In order to estimate the scattered light intensity, we can use (4). However, the 2D nature of the scattering volume should be essentially taken into account. In this case, the density fluctuations can be expressed in the Fourier representation as

$$\rho=\sum_{\mathbf{q}}e^{i(q_y y+q_z z')}\rho_{\mathbf{q}}(t)\delta(x'), \tag{5}$$

where $\mathbf{q}$ belongs to the 2DEG plane. In (5), rotation around the y axis was performed as follows (Fig. 2):

$$z'=z\cos(\beta)+x\sin(\beta), \qquad x'=-z\sin(\beta)+x\cos(\beta). \tag{6}$$

The coordinate z' is directed orthogonally to the AB edge in the 2DEG plane; x' is orthogonal to this plane. Substituting (5) and (6) and (1) and (3) into (4) and integrating over time and space coordinates, we arrive at the expression for the intensity of Stokes component as

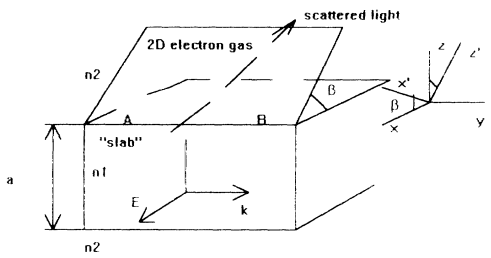

FIG. 2. The geometry of EFRS from the 2D electron gas.

$$\tilde{I}_H(\omega)=\rho_e L_{AB}\int\frac{dq_z}{2\pi}\frac{2\eta^2 S(q_z,q_y)\pi\delta(\omega+\varepsilon_{\mathbf{q}})}{(\delta\sin\beta)^2+(q_z-\Delta k)^2}\cos^2(\beta),$$
$$\Delta k\equiv k'_z\sin\beta-k'_x\cos\beta, \quad q_y=k'_y-k_y, \tag{7}$$
$$\eta\equiv\cos[(a/2)\sqrt{\varepsilon(\Omega/c)^2-k_y^2}],$$

where δ and k_y are solutions of (2) and it was taken into account that for Stokes component at $T=0$ we have

$$\int dt\,e^{-i\omega t}\langle\rho_{\mathbf{q}}(t)\rho_{\mathbf{q}}(0)\rangle=\rho_e S_{\mathbf{q}}\pi\delta(\varepsilon_{\mathbf{q}}+\omega), \tag{8}$$

with $S_{\mathbf{q}}$ and ρ_e being the static structure factor and the average density of electrons, respectively. In (7), L_{AB} stands for the length of the AB edge (see Fig. 2). Since we assumed that the beam has an infinite size in the x direction, (7) is valid only when $\beta>\delta/d$, where d is the size of the beam. The extra factor of $\cos^2(\beta)$ in (7) appears due to the fact that only the parallel component of the electric field is essential for the scattering.

For comparison, let us write down the expression for the RS intensity measured in [10] in the backscattering geometry. In this case, we have

$$\tilde{I}_B(\omega)\cong A\rho_e S_{\mathbf{q}}\delta(\omega+\varepsilon_{\mathbf{q}}), \quad \mathbf{q}=\mathbf{k}'_p-\mathbf{k}_p, \tag{9}$$

where A stands for the area of the spot illuminated by the incident light and $\mathbf{k}'_p,\mathbf{k}_p$ are the wave vector components in the 2DEG plane of the scattered and incident light, respectively. For the structure factor $S(\mathbf{q})$ of the 2DEG, one may employ the expression [2] from the "single mode approximation":

$$S_{\mathbf{q}}=\mathbf{q}^2/2m_e\varepsilon_{\mathbf{q}}, \tag{10}$$

where m_e is the electron mass, and hence after $\hbar=1$. In the case of small $|\mathbf{q}|$, the contribution of the magnetoroton to $S_{\mathbf{q}}$ turns out to be negligibly small ($\sim q^4$) [2]. However, for q being close to the inverse magnetoroton wavelength λ_r^{-1}, Eq. (9) provides a good description of the density fluctuations, caused by magnetorotons.

We should note that the values of transferred momentum $|\mathbf{q}|$ in (9) are small compared to the typical magnetoroton inverse wavelength λ_r^{-1}. At the same time, in the case of (7), the integration over q_z is performed. Therefore, we obtain a considerable contribution from the region $q_z\sim\lambda_r^{-1}$. In order to demonstrate this, let us take

the excitation spectrum in the well-known form

$$\varepsilon_{\mathbf{q}} \approx \Delta_r + \frac{(\mathbf{q}-\lambda_r^{-1})^2}{2m^*} \tag{11}$$

first introduced by Landau for ^{4}He [1], with Δ_r, m^* being some suitably chosen parameters. Then, a substitution of (10) and (11) into (7) yields

$$\tilde{I}_r(\omega) \approx L_{AB}\rho_e \frac{\eta^2}{2m_e} \frac{\sqrt{2m^*}}{|\omega|\sqrt{|\omega|-\Delta}}, \quad \omega \le -\Delta, \tag{12}$$

where we took into account that $\lambda_r^{-1} \gg \max(\delta, \Delta k)$. We see that the roton contribution turns out to be strongly asymmetric, with the inverse square root singularity.

Making use of the result [2], one can obtain

$$1/2m^* \cong [\Delta(0)-\Delta_r]\lambda_r^2 \tag{13}$$

to be substituted into (12), where $\Delta(0)$ stands for the gap of the Laughlin liquid at $q=0$. From [2], one can find

$$\Delta(0) \cong 0.15\frac{e^2}{\varepsilon l_H}, \quad \Delta_r \cong 0.055\frac{e^2}{\varepsilon l_H} \cong \tfrac{1}{3}\Delta(0), \tag{14}$$

where e stands for the electron charge and l_H is the magnetic length. Substituting (13) into (12), we obtain the integrated intensity of EFRS as

$$\tilde{I}_H = \int d\omega \tilde{I}_H(\omega) \cong \frac{\pi}{2} L_{AB}\rho_e \frac{\eta^2}{2m_e\lambda_r} \frac{1}{\sqrt{\Delta_r[\Delta(0)-\Delta_r]}}. \tag{15}$$

The integral intensity in the backscattering geometry [5,10] may be estimated from (9) as

$$\tilde{I}_B \cong d^2\rho_e \mathbf{q}^2/2m_e\omega_c, \tag{16}$$

where ω_e is the cyclotron frequency. The ratio of these two contributions turns out to be

$$R_H = \frac{\tilde{I}_H}{\tilde{I}_B} \cong \frac{L_{AB}}{d^2} \frac{\eta^2\omega_c}{\lambda_r \mathbf{q}^2} \frac{1}{\sqrt{\Delta_r[\Delta(0)-\Delta_r]}}. \tag{17}$$

Choosing $q \cong 2\pi/\lambda$, with λ being the wavelength of light, and employing the estimates (16) and (17) as well as $\lambda_r \cong l_H$, $\eta \cong 1$, we obtain

$$R_H \cong 0.1\frac{L_{AB}\lambda}{d^2} \frac{\lambda}{l_H} \frac{\omega_c}{e^2/\varepsilon l_H}. \tag{18}$$

Since $\lambda \ge 100 l_H$, $\omega_c > e^2/\varepsilon l_H$, $d \sim 10^1$–$10^2\lambda$, and L_{AB} is a macroscopic length, one may conclude that the EFRS intensity from 2DEG can be much greater than the RS in the backscattering geometry.

In order to observe the gap excitations, a resonant RS technique was applied in [5,10]. Since in the EFRS the intensity is considerably enhanced, one may use nonresonant Raman scattering. In this case, one can avoid troubles with mixing of the RS and luminescence.

As mentioned above, the 3D rotons may be observed by the EFRS as well. The short-wave rotons ($\lambda_r \le 10^{-7}$) may be detected by neutron scattering, as was done for ^{4}He [11]. For larger λ_r, probing of the single-roton spectrum by neutrons would encounter the well-known difficulties. Therefore, EFRS may also be valuable to study this kind of roton. Let us demonstrate that the roton contribution to inelastic scattering intensity is also significant in the 3D case.

As an example, let us consider the EFRS from liquid ^{4}He at $T \to 0$. In this case, however, the acoustic phonons provide an additional contribution to the EFRS. We will show that this contribution does not exceed the roton contribution and both of them can be identified. The excitation spectrum can be taken in the form ([1])

$$\omega_q = \begin{cases} uq, & q \to 0, \\ \Delta + \dfrac{(q-q_0)^2}{2M^*}, & q \cong q_0, \end{cases} \tag{19}$$

where u stands for the sound velocity, Δ is a roton gap, and q_0 is the roton wave vector; M^* denotes the ^{4}He roton effective mass. Using (4) analogously to (7), we obtain for the Stokes component of scattered radiation

$$\tilde{I}(\omega) = A\int_{-\infty}^{+\infty} \frac{dq_z}{2\pi} \frac{2\eta^2}{\delta^2+(q_z-k_\perp')^2} \frac{\rho_0(q_z^2+\mathbf{q}^2)}{M\omega_q} \times \pi\delta(\omega+\omega_q), \tag{20}$$

where the structure factor for ^{4}He was taken in the form (10), with the electronic mass and the averaged density replaced by ^{4}He atomic mass M and density ρ_0; A stands for the area of the boundary surface. For $\omega < \Delta$ in (20), the upper line of (9) should be used. It corresponds to the Mandelstam-Brillouin feature in the bulk RS. For this contribution, we have

$$I_s(\omega) = \frac{A\rho_0\eta^2}{2Mu} \frac{\omega^2}{\sqrt{\omega^2-(uq)^2}} \left[\frac{1}{\delta^2u^2+[\sqrt{\omega^2-(uq)^2}-k_\perp']^2} + \frac{1}{\delta^2u^2+[\sqrt{\omega^2-(uq)^2}+k_\perp']^2} \right], \tag{21}$$

where $-\Delta < \omega < -u|\mathbf{q}|$; δ, k_y, and η have the same meaning as in (7). For $\omega < -\Delta$, the roton part of spectrum (18) gives an additional contribution. Making use of the inequality $\delta \approx |\mathbf{q}| \approx k_\perp' \ll q_0 \approx 10^8$ cm^{-1}, the intensity of scattering by rotons can be expressed from (20) as

$$\tilde{I}_r(\omega) \approx \frac{A\rho_0\eta^2}{2M} \frac{\sqrt{2M^*}}{|\omega|\sqrt{|\omega|-\Delta}}, \quad \omega \le -\Delta. \tag{22}$$

It is worth noting that this contribution does not contain any smallness in the ratio $1/\lambda q_0 \ll 1$. From (21) and (22) one can see that both features have the inverse square

root singularity in ω near the thresholds $u|\mathbf{q}|$ and Δ, respectively. Note that, as shown in [12], the second-order RS due to a pair of rotons in ^{4}He also has a square root singularity, with the threshold twice the roton gap.

Let us compare the integrated intensities $I_s = \int d\omega \times I_s(\omega)$ and $I_r = \int d\omega\, I_r(\omega)$ of these features. An integration yields

$$I_s = \frac{A\rho_0\eta^2}{Mu}\int_{-\infty}^{+\infty} dq_z \frac{\sqrt{q_z^2+\mathbf{q}^2}}{\delta^2+(q_z-k'_\perp)^2},$$

$$I_r \cong \frac{A\rho_0\eta^2}{M}\int_{-\infty}^{+\infty} dq_z \frac{1}{\Delta+q_z^2/2m^*} = \frac{A\rho_0\eta^2}{M}\pi\left(\frac{2M^*}{\Delta}\right)^{1/2}. \tag{23}$$

The main contribution to I_s comes from the region $|q_z - k'_\perp| \le \delta$. Therefore, one obtains

$$I_s \cong \frac{A\rho_0\eta^2}{Mu}\pi\frac{\sqrt{k'^2_\perp+\mathbf{q}^2}}{\delta}. \tag{24}$$

Using (23), we can obtain the ratio R of EFRS by rotons to that by phonons:

$$R \equiv \frac{I_r}{I_s} \cong \frac{u\delta}{\sqrt{k'^2_\perp+\mathbf{q}^2}}\left(\frac{2M^*}{\Delta}\right)^{1/2}. \tag{25}$$

As was mentioned above, the quantity δ is of the same order of magnitude as $k'_\perp$ and $|\mathbf{q}|$. Therefore, we can estimate R in (24) as

$$R \cong \left(\frac{M^*u^2}{\Delta}\right)^{1/2}, \tag{26}$$

where $u \cong 10^5$ cm/s, $m^* \cong 10^{-24}$ g, $\Delta \cong 1$ K. Substitution of these values into (25) gives $R \cong 10$. It implies that the roton contribution to the scattering intensity should be about 1 order of magnitude stronger than the one due to acoustic phonons.

We should note that the total intensity is proportional to the effective scattering volume V_{eff}. In the case of bulk scattering, we have $V_{\text{eff}}^{\text{bulk}} \cong Ld^2$, where L stands for the length of the sample and d is the beam diameter. In the case of evanescent scattering, $V_{\text{eff}} \cong Ld\delta$. Therefore, the ERS is reduced by a factor of $\sim\delta/d$ in comparison with the bulk Mandelstam-Brillouin intensity. Since d is of the order of tens of the wavelength, we cannot expect any serious reduction of the EFRS in comparison to the bulk Mandelstam-Brillouin line.

The EFRS may also be useful in studying nonliquid substances, where the roton peculiarity of the quasiparticle spectrum would rather be nonisotropic and assigned to particular points of the Brillouin zone. In this case, the EFRS intensity may have the inverse square root singularity as a function of frequency near the roton creation threshold. This effect should be much stronger than the usual RS square root singularity in the presence of impurities. This happens due to the quasi-1D geometry of the evanescent field.

Therefore, we conclude that the EFRS on roton-type peculiarities of the spectrum gives a considerable contribution. It may be applied to the 2D electron gas in a high magnetic field in experimental circumstances close to those used recently by Pinczuk and collaborators [5,10]. It also seems to be possible to observe the first-order EFRS by rotons in the 3D case for different types of excitations, particularly the rotons in liquid ^{4}He.

We are grateful to Professor H. Z. Cummins for drawing our attention to Refs. [6,12]. One of us (A.B.) is supported by the Fellowship from the Graduate Center of CUNY.

[1] E. M. Lifshitz and L. P. Pitaevsky, *Statistical Physics* (Pergamon, Oxford, 1981), Pt. 2.
[2] S. M. Girvin, A. H. MacDonald, and P. M. Platzman, Phys. Rev. Lett. **54**, 581 (1985); Phys. Rev. B **33**, 2481 (1986).
[3] S. H. Simon and B. I. Halperin, Phys. Rev. B **48**, 17368 (1993).
[4] R. A. Cowley, Adv. Phys. **29**, 1 (1980).
[5] A. Pinczuk, J. P. Valladares, D. Heiman, A. C. Gossard, J. H. English, C. W. Tu, L. Pfeifer, and K. West, Phys. Rev. Lett. **61**, 270 (1988).
[6] T. J. Greytek and J. Yan, Phys. Rev. Lett. **22**, 987 (1969).
[7] G. A. Massey, Appl. Opt. **23**, 658 (1984); U. Dürig, D. W. Pohl, and F. Rohner, J. Appl. Phys. **59**, 3318 (1986); R. C. Reddick, R. J. Warmack, and T. L. Ferrell, Phys. Rev. B **39**, 767 (1989).
[8] J. C. Selser, K. J. Rotschild, J. D. Swalen, and F. Rondelez, Phys. Rev. Lett. **48**, 1690 (1982); K. H. Lan, N. Ostrovsky, and D. Sornette, Phys. Rev. Lett. **57**, 17 (1986); Jun Gao and Stuart A. Rice, J. Chem. Phys. **90**, 3469 (1989); Martin Copic, Cheol Soo Park, and Noel A. Clark, Mol. Cryst. Liq. Cryst. **222**, 111 (1992).
[9] L. D. Landau, E. M. Lifshitz, and L. P. Pitaevsky, *Electrodynamics of Continuous Media* (Pergamon, Oxford, 1984), 2nd ed.
[10] A. Pinczuk, B. S. Dennis, L. N. Pfeifer, and K. West, Phys. Rev. Lett. **70**, 3983 (1993).
[11] A. D. B. Woods and R. A. Cowley, Phys. Rev. Lett. **24**, 646 (1970).
[12] J. W. Halley, Phys. Rev. **181**, 338 (1969); M. J. Stephen, Phys. Rev. **187**, 279 (1969).